*EVS24*
*Stavanger, Norway, May 13-16, 2009*

# Low-pass Filtered Power-flow Control in Series Hybrid Electric Vehicle

Matti Liukkonen [1], Ari Hentunen [1] Jussi Suomela [2], Jorma Kyyrä [1]

[1] *M. Liukkonen is with Helsinki University of Technology, Department of Electrical Engineering, P.O. Box 3000, FI-02015 TKK, Finland (e-mail: matti.j.liukkonen@tkk.fi; ari.hentunen@tkk.fi; jorma.kyyra@tkk.fi).*

[2] *J. Suomela is with Helsinki University of Technology, Department of Automation and Systems Technology, P.O. Box 5500, FI-02015 TKK, Finland (e-mail: jussi.suomela@tkk.fi)t*

## Abstract

This paper presents a low-pass filtered power-flow control strategy for a series hybrid electric vehicle (S-HEV) with an energy buffer. The proposed control aims to decrease the maximum power values from the primary energy source and, secondly, to reduce the engine-generator dynamics at sudden load changes (from low loads at low speed to high loads). In case of variable speed diesel generator (VSDG) set downsizing reduces the emissions and the fuel consumption. The proposed control strategy is introduced with two different driving cycles, both, for the urban and the sub-urban areas. The energy losses, caused by the energy buffering, and the sizing of heavy duty vehicle's series hybrid drive train are gained as a result.

*Keywords: Low-pass filtered power-flow control, heavy duty vehicles, plant optimization, series hybrid electric vehicle, simulation*

## 1 Introduction

THIS study is part of a duty vehicles hybridization project. Heavy duty vehicles typically have very machine and task specific cycles, which are difficult to generalize. Therefore, the well known Braunschweig and New European Driving (NEDC) cycles have been used in order to provide new information about power losses in supercapacitor (SC) buffered series HEV driveline. The study, which is made for the duty machines, can also be utilized for heavy duty road vehicles such as trucks and busses.

Usefulness of the hybrid electric driveline depends on the load cycle. Therefore, this paper presents a low-pass filtered power-flow control [5], [7]-[9], [11], [16] with two different load profiles, which argues for both convenient and inconvenient cycles. As a result, the study offers confirming data for reducing the size of the primary energy source compared to other research [8], as well as, sizing and power losses, in both, in the SC and in the dc/dc converter of the system [6].

It has been shown that bad dynamical properties of the system for the VSDG, as in conventional drive train, can be considerably improved by implementing power electronic converters with an energy buffer [12]. The low-pass filtered power-flow control reduces dynamic requirements from the primary energy source.

The presented low-pass filtered power-flow control also seeks methods to reduce the deep discharge cycles from the SC, which causes limited life-time in very cyclic applications. In order to achieve sufficient lifetime of supercapacitors, it should be avoided to use the full operation range of the SC (50% to 100% state of charge, SOC), which has a limited lifetime of 1 million cycles.

# 2 Introduction

## 2.1 Topology

The series hybrid drive train is presented in Fig. 1. The VSDG generates ac current to the active front end converter (AFE), which converts the ac current to the dc current and stabilizes the dc link voltage. The AFE regulates the dc link voltage to 650 V in the proposed system. The energy storage (ES), in this case a supercapacitor module, is connected via the dc/dc converter to the dc link. The inverter is connected to the dc link and is used directly from Power Management System (PMS) for the traction control purposes.

The proposed variables for the power-flow control are the load power to the inverters, the speed of the vehicle, the dc link voltage and the energy storage voltage [9], [10]. The load power can be considered as a measured or as a feedforward value [4]. The control signals for the power-flow control are the dc link voltage reference, which would be controlled from the PMS, feedforward power flow for the AFE, the dc/dc converter's current and the speed of the VSDG [2] [12]. VSDG is controlled within optimal operation area [14] [16]. The system topology, the control signals and variables are shown in Fig. 1.

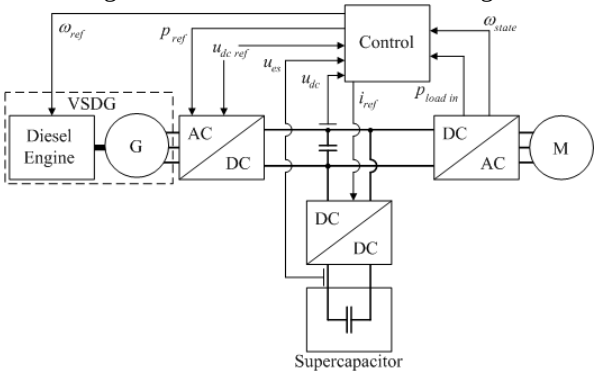


**Fig. 1 The system topology, the control signals and control variables for the supercapacitor buffered series-hybrid electric transmission.**

## 2.2 Propulsion power in the Driving Cycles

The required propulsion power from the electric transmission is determined based on the system constraints as maximum acceleration, rated and maximum vehicle velocity, and vehicle gradability. The propulsion power calculation is straightforward with the following equations. First, the total traction force is solved:

$$F(t) = C_0 mg + \frac{1}{2}\rho C_d A_F v(t)^2 + ma(t) \quad (1)$$

where $F(t)$ is the traction force as a function of time, $C_0$ is the static friction coefficient, $m$ is the mass, $g$ is the gravitation, $\rho$ is the air density, $C_d$ is the air friction coefficient, $A_F$ is the cross-sectional area, $v(t)$ is the current velocity according to time, and $a$ is the acceleration as a function of time. Then, the propulsion power $P(t)$ as a function of time is:

$$P(t) = F(t)v(t) \quad (2)$$

Therefore, solving of the propulsion power starts from the driving cycle, which gives the current speed and the acceleration as a function of the time. In the simulations we use the NEDC and the Braunschweig cycles to demonstrate the behavior of the presented control, as in reference [7]. Table I shows the environment and the vehicle parameters used to simulate the required propulsion power.

TABLE I
Environment and vehicle parameters in simulations [1]

| Symbol | Quantity | Value |
|---|---|---|
| $C_0$ | static friction coefficient | 0,013 $s^2/m^2$ |
| $m$ | mass | 10 000 kg |
| $g$ | gravitation | 9,81 $m/s^2$ |
| $\rho$ | air density | 1,29 $kg/m^3$ |
| $C_d$ | air friction coefficient | 0,3 |
| $A_F$ | cross-sectional area | 8 $m^2$ |

Fig. 2 illustrates the speed and the required propulsion power for the NEDC and Fig. 3 represents the same variables for the Braunschweig cycle. These figures depict how the propulsion power reaches its highest values in the end of the acceleration and the regenerative power at the start of the deceleration.

The NEDC represents both, the urban and the sub-urban area cycles. As from the Fig. 2 can be seen, the change point of the urban and the sub-urban areas in the NEDC is in the 800 seconds. The Braunschweig cycle simulates only the urban area operation with shorter accelerations and decelerations contrary to NEDC.

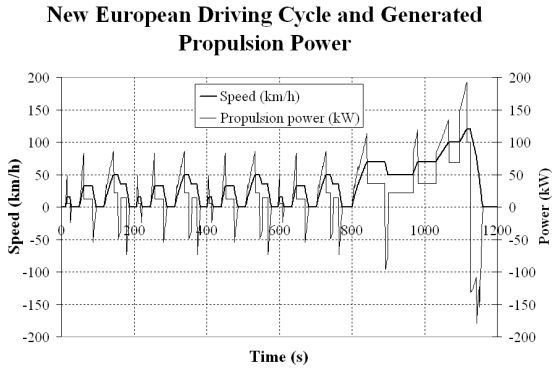


**Fig. 2 The New European Driving Cycle and the required propulsion power (duration 1160 s, length 11.0 km, average speed 34.2 km/h, max speed 120 km/h, share of idle 22.4%).**

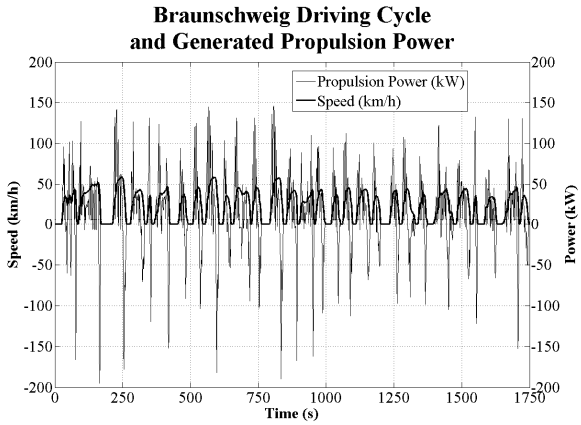


**Fig. 3 The Braunschweig driving cycle and the required propulsion power (duration 1740 s, length 10.9 km, average speed 22.5 km/h, max speed 58.2 km/h, share of idle 25%).**

The following simulations are made to illustrate how the maximum propulsion power can be reduced with the low-pass filtered power-flow control in different driving cycles, and which are its drawbacks.

Besides the propulsion power calculated from the driving cycles, the simulated cases are assumed to consume constant power to auxiliary devices of the vehicle. Constant power is simply added to propulsion power. In these simulation cases proper constant power consumption would be e.g. 10 kW, which is later used in the simulations.

## 2.3 Power losses in simulations

The power transfer efficiencies have a significant role in order to define the usefulness of S-HEV driveline. In this paper, the power losses deriving from power-flow filtering in dc/dc converter and supercapacitor module are considered. This is realized with measurement based efficiency maps from the dc/dc converter and ESR value of a commercial supercapacitor module. The power losses in other converters and electric machines of studied system are left out of the scope, though; they are still modeled with the same hybrid simulation modeling principle.

Inverters, rectifiers and traction motors, are modeled based on hybrid simulation modeling of converters and electric machines. These models are built with the efficiency maps received from the manufacturer. In hybrid simulation models, the transferred power through the power train is scaled with the efficiency value of the operation point of the device in question.

Simulations concentrate only on system level power transfer. Therefore, typical behavior of the supercapacitors electrochemical characteristics is left out of consideration and simulations only consider electrical characteristics of the energy storage. Although supercapacitors resistance and capacitance are state of charge dependent, supercapacitor modules are simulated with constant equivalent series resistance and capacitance [13]. Also, leakage currents of supercapacitors are neglected.

## 2.4 Hybrid Simulation model of the dc/dc converter

Dc/dc converter's transient behavior is neglected in the simulations, which causes a small error to the supervisory control simulations by the step response of modern dc/dc converter. Therefore, dc/dc converters are assumed to be ideal and the simulation steps are pushed longer.

The power losses during the converter's operation are defined with the measured efficiency data. Efficiency values from the converter's different operation points are used to calculate the power losses in the dc/dc converter and in the SC module during the energy buffering [3]. In the simulations, when operation point exceeds the limit of the efficiency map, the end value of the map is used. Preceding approach is widely called as a hybrid simulation model.

Fig. 4 shows the efficiency map of the buck-boost dc/dc converter as a function of the transferred current and the ratio between upper and lower voltage levels. The figure represents charge operation and it is based on the measurements done for the dc/dc converter which has interleaved inductor phases and 120 amps nominal current.

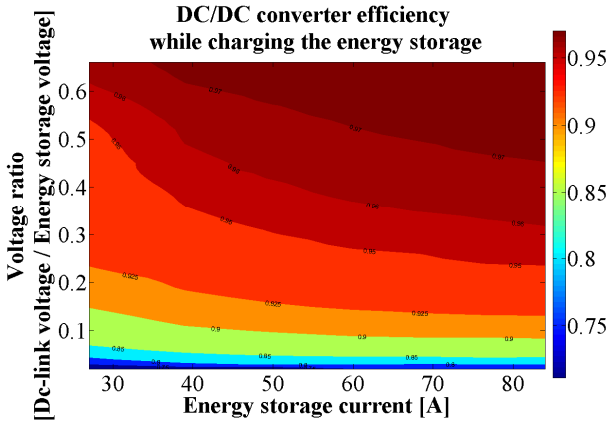


**Fig. 4 The measured efficiency map of the dc/dc converter during charge operation.**

The total power transfer efficiency from the dc link side is solved from the efficiency maps of the charge and discharge operations of the dc/dc converter, and also with the equivalent series resistance (ESR) of the supercapacitor module. One efficiency map of the energy storage according to ESR losses is shown in Fig. 5. The efficiency map from the ESR losses is calculated with the equation:

$$\eta = \frac{u_{sc} - R_{ESR} * i_{sc}}{u_{sc}}$$

where $\eta$ is the efficiency, $u_{sc}$ is the voltage of the SC module, $R_{ESR}$ is the equivalent series resistance attained from the datasheet [15] and $i_{sc}$ is the current of the SC module.

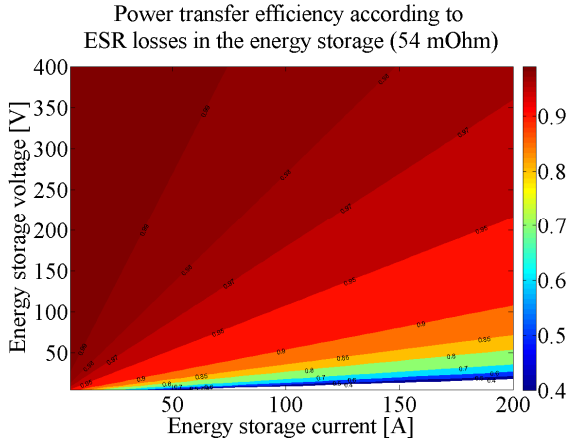


Fig. 5 The power transfer efficiency according to ESR losses in the energy storage.

Accuracy of solving the power losses in a supercapacitor module is reduced when the losses are calculated only with ESR value of the dc resistance. This is because the capacitance of a supercapacitor is very frequency dependent [13]. Therefore, assumption with supercapacitor power losses modeling is that converters transfer only dc current and power losses caused by converters switching frequencies are neglected. So, the simulated power losses in the supercapacitor module are considered to be the minimum that can be realized. Previous further speeds up system level modeling, while more accurate modeling of losses with higher frequency components make simulations unnecessary complicated.

Fig. 6 represents the total power transfer efficiency of the energy buffering. Figure is done by multiplying efficiency maps from the dc/dc converter and from the supercapacitor module with each other. So, the figure takes into account charge and discharge operations of the dc/dc converter and the ESR of the supercapacitor module. This figure is based on both theoretically calculated and experimentally measured efficiency values.

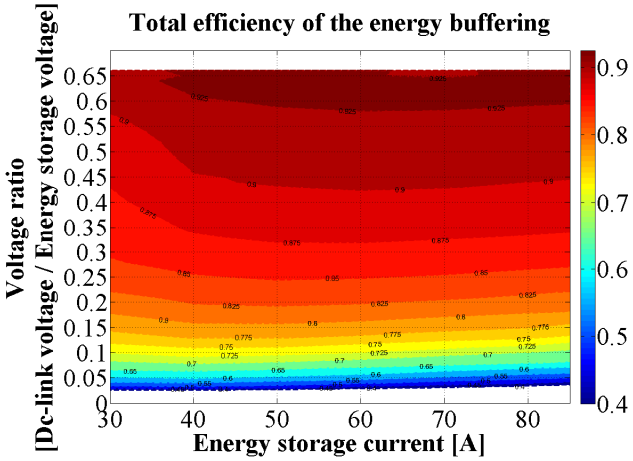


Fig. 6 The total power transfer efficiency map from the dc link side according to theoretical calculations and experimental measurements.

# 3 Presented power-flow control

## 3.1 Power-flow control in the dc link

The low-pass filtered power-flow control, which is previous presented in studies [5], [7]-[9], [11], can be implemented above the system shown in Fig. 1. It can be generalized into two parts. The first is the peak power shaving control algorithms and the second is the low-pass filtered power-flow control, which is build on the top of the first one. The low-pass filtered power-flow control simply makes the peak power shaving limits to move.

### 3.1.1.1 The Peak Power Shaving control

The proposed peak power shaving control is based on the minimum and the maximum power limits. These limits can also be used to specify the converter's current direction. The power limits are compared with the subtraction to the measured load power, and the result is saturated either with the normal or with the dynamic saturation. The minimum power limit is creating an inverse of the correct power buffering value; therefore it is needed to take absolute value from power buffering signal. The saturation values for the peak power shaving are from the zero to the maximum desired, and for the power buffering from the maximum buffered power to the power which triggers the buffering. The previous signals are next divided by the state value of the dc link voltage for to achieve the peak shaving and buffering current references. By adding them together, we attain dc/dc converter's current reference in the dc link side. Then, the error value from dc link's voltage is added to the current reference with the proportional gain for to more stabilize the dc links voltage. In the end, the current reference is shifted to ES's voltage level, in case where the dc/dc converter is designed to control the current in the ES's side.

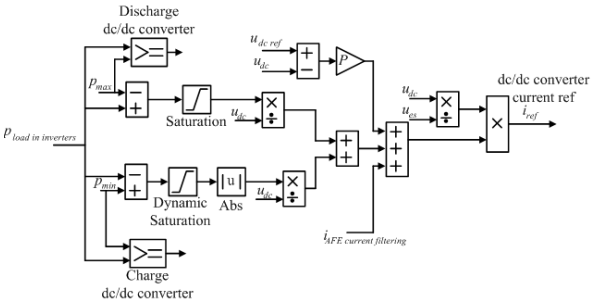


**Fig. 7 The Peak Power Shaving control.**

### 3.1.1.2 The low-pass Power-flow control

The low-pass power-flow control, which is shown in Fig. 8, is built on the top of the peak power shaving control. In the proposed control strategy, the idea is to make the maximum and the minimum power limits to move as a function of the load power and the voltage of the ES.

First, the state value of the load power is determined and brought to the supervisory control. Second, the discrete finite impulse response (FIR) filter averages the load power. This could also be made with several filters with different time constants [11]. According to the simulations it is suggested that the power is averaged with the time of the longest acceleration during the driving cycle [7]. In this paper filtering is done with only one time constant, which is 20 seconds. Third, the filtered power is weighted with 2 - 1/75000*$p_{filtered}$ function. This function priories the power buffering to take place in low loads instead of times of high loads.

In contrast to filtered load power value, energy storage's voltage determines the power level, which needs to be generated by the primary energy source. Previous is realized with a function, which gets high power values at low energy storage's SOC and vice versa. In the simulations this function was formulated as 75000 – 750/5*$v$, and it is only scaled with maximum energy storage's voltage level value between different simulation cases. In principle, this function creates power limit plane which defines either to cut peak powers or buffer the power from the VSDG. In addition, weighted function from energy storages voltage is filtered with 2 seconds time constant, which is also used to filter the variation of the power limit plane.

In the low-pass filtered power-flow control, the next step is to multiply prioritization function from the filtered load power and the power level created by energy storage's voltage. The result creates a weighted power limit plane as a function of filtered load power and energy storages voltage. Then; the hysteresis are added to the created power limit plane. These hysteresis are used to create delay between dc/dc converter's charging and discharging control signals. After hysteresis, control schemes from Fig. 7 and Fig. 8 interconnect. The proposed power limit plane has built-in maximum voltage limit for the SC.

Fig. 8 also presents algorithm, which filters more the AFE current. This AFE current filtering is also added to dc/dc converter current reference, shown in fig. 7, with the proportional gain value. The AFE current filtering component is calculated from the state value of the AFE current, filtered value of the AFE current and with multiport switch, which takes in consideration of present current direction in dc/dc converter. Filtering of the AFE current was done with 20 seconds time constant.

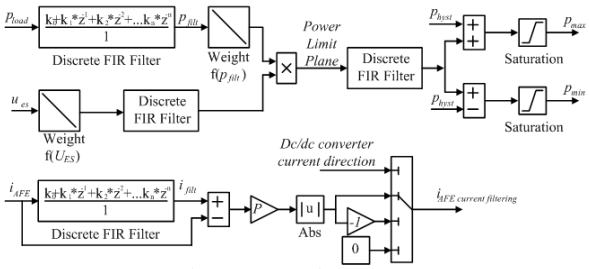


Fig. 8 The Low-pass filtered power-flow control algorithm.

The system without a load is driven automatically to high SOC value, if the power limits are kept high compared to the present state of the load power. This provides SOC to be adequate for the next acceleration. Fig. 9 presents the PLP set by the weighted variables.

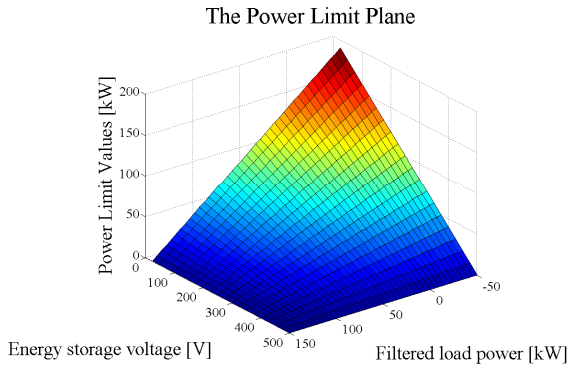


Fig. 9 The power limit plane set by weighted values from energy storage's voltage and the filtered power.

Table II presents the parameter values which were used in the introduced control.

TABLE II
Current controller parameters in the simulations

| Symbol | Quantity | Value / function |
|---|---|---|
| $P$ | Proportional gain in fig. 7 | 0,25 |
| $P$ | Proportional gain in fig. 8 | 0,5 |
| $i_{ref}$ | Dc/dc converter's current ref in the energy storage side | -- |
| $f(p_{filt})$ | The weighting function for the filtered power | $2 - 1/75000 * p_{filtered}$ |
| $f(U_{ES})$ | The weighting function for the energy storage voltage | $75000 – 750/5 * v$ |

## 3.2 The flowchart of the proposed power-flow management

Fig. 10 represents the startup flowchart for the proposed power-flow management. In the beginning, the system is in rest. After the auxiliary power is switched on, the VSDG is started and the supercapacitor module is charged to the specified level. Then, the dc link voltage is regulated with the AFE to 650 V level. After the activation of the dc link voltage regulation, the low-pass power-flow control begins to operate.

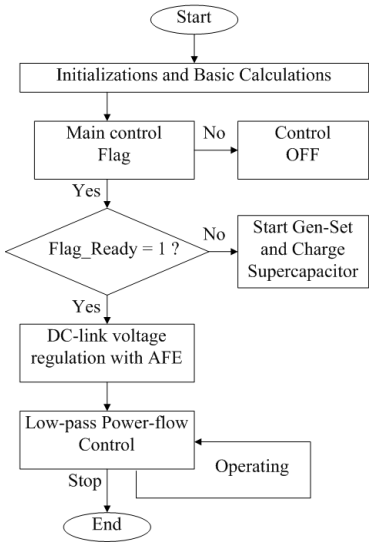


**Fig. 10 The flowchart of the proposed power-flow management algorithm.**

## 3.3 Control of Active Front End converter in the simulations and generation of operation points of the Diesel Engine

In the proposed control, the dc link voltage is stabilized with the active front end converter. AFE get its control signals from the supervisory control as a dc link voltage reference and as a transferable power to the dc link. The voltage reference was set to 650 V during the simulations and the power reference was calculated from the static traction power component of equations 1 and 2. So, feedforwarded power reference was calculated without the term, which included acceleration.

In the used AFE simulation model, limited maximum current as a function of the generator speed specifies the maximum counter torque of the VSDG simulation model. As a VSDG simulation model was used one-dimensional model of the diesel-engine. The difference between the VSDG maximum torque and the limited counter torque of the AFE define dynamical torque, which is used for the speed change of the VSDG. The control strategies of the variable speed diesel generating systems were further studied in [14].

The speed reference for the VSDG can be obtained with several different strategies [14]. Proposed control in the simulations formulates the VSDG speed reference from the transferred power of the AFE. Created operation points in one simulation of this control strategy are shown in Fig. 11. Figure presents generated power of the VSDG as a function of the speed of the VSDG with red crosses. Period between operation points was half second. In

addition, the figure includes maximum power curve of the VSDG simulation model (black curve) the maximum power of AFE specified by its counter torque (blue curve) and specific fuel consumption curves of the used VSGD simulation model.

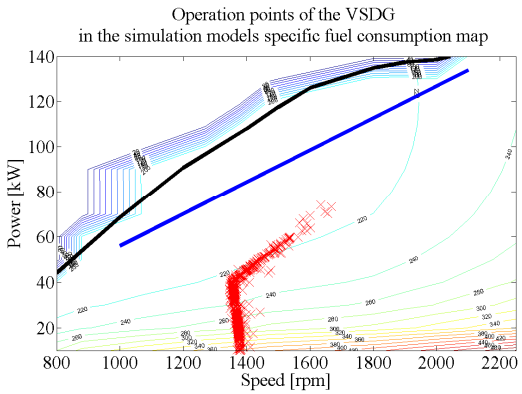


Fig. 11 The variable speed diesel generator operation points at the start of one simulation case with Braunschweig driving cycle and 31,5 F energy storage.

Operation points of the VSDG during simulation are determined by equation:

$$\frac{d\omega}{dt} = \frac{T - T_L}{J} \qquad (5)$$

where $d\omega/dt$ is differential speed change, $T$ is torque of the VSDG, $T_L$ is counter torque of the AFE and J is inertia of the gen-set shaft. In the simulations, inertia of the simulated VSDG was assumed to be 1 kgm$^2$ and the initial speed of the VSDG was 1400 rpm.

# 4 Simulations

The simulations are done with the 5 combinations of the capacitance value of the SC module and its maximum voltage level. The results from the simulations are tabulated and simulation figures from Case I are shown. Table III represents the SC dimensioning in different simulation cases. Energy storage's nominal values are based on manufacturer data. In these simulation cases supercapacitors are considered as built-in modules, which include cells, connections between cells, voltage balancing circuits, packaging and cooling [15].

TABLE III
Dimensions of the energy buffer in different simulation cases [15]

| Quantity | Values Case I | Values Case II | Values Case III | Values Case IV | Values Case V |
|---|---|---|---|---|---|
| Capacitance (F) | 31,5 | 42 | 63 | 12,6 | 25,2 |
| ESR (mΩ) | 34 | 25,5 | 17 | 85 | 42,5 |
| Maximum Voltage (V) | 500 | 375 | 375 | 625 | 625 |
| Weight (kg) | 464 | 348 | 522 | 290 | 580 |
| Usable energy (kWh) | 0,82 | 0,62 | 0,92 | 0,512 | 1,03 |
| Continuous current (A) | 300 | 300 | 450 | 150 | 300 |
| Maximum current (A) | 1500 | 1500 | 2250 | 750 | 1500 |
| Modules (series / parallel) | (4 / 2) | (3 / 2) | (3 / 3) | (5 / 1) | (5 / 2) |
| Cells (series / parallel) | (188 / 2) | (141 / 2) | (141 / 3) | (235 / 1) | (235 / 2) |
| Initial Voltage (V) | 450 | 337,5 | 337,5 | 562,5 | 562,5 |

* The efficiency map of the dc/dc converter is extrapolated in simulation cases where the maximum voltage value rises higher than 400 V.

The simulation figures present the total load current, the dc/dc converter current, the AFE current, the energy storages voltage and the dc link voltage, which are variables of proposed control algorithm.

## 4.1 The simulation figures with NEDC

The load current, which was drawn from the dc link, was solved with equations 1, 2 and with dc link voltage state. In addition, current change rate were limited not to reach infinite value and to imitate proper ramp times of power converters. The load current, in case I, is shown in Fig. 12 during three rounds of ECE cycle.

### 4.1.1.1 Simulations with the ECE cycle

Figures 12 – 15 presents three rounds of simulations with ECE cycle. This means 600 seconds long simulation.

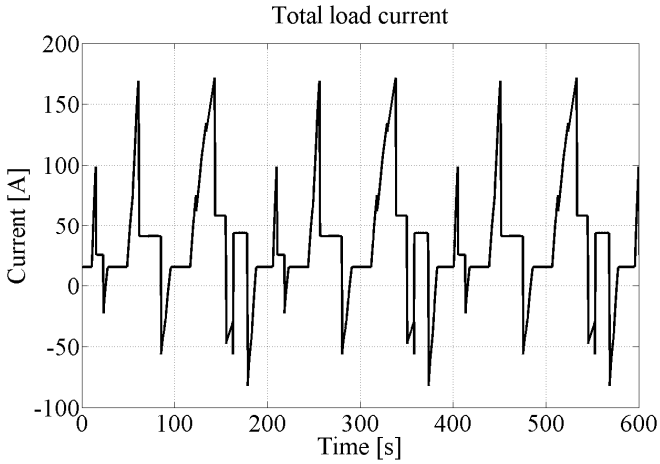


Fig. 12 The simulated load current, which was solved from the traction power and from constant power consumption during three rounds of ECE cycle.

In this study presented control scheme creates dc/dc converter current, which is shown in Fig. 13. This dc/dc converter current is presented in energy storage voltage level.

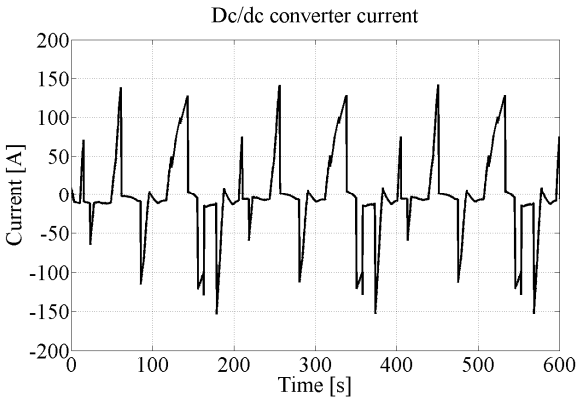


Fig. 13 The simulated dc/dc converter current, in case I, during three rounds of ECE cycle.

The simulated active front end converter current in the dc bus is shown in fig. 14. The figure shows a result of low-pass power filtering with dc/dc converter and simultaneous dc link voltage regulation of the AFE.

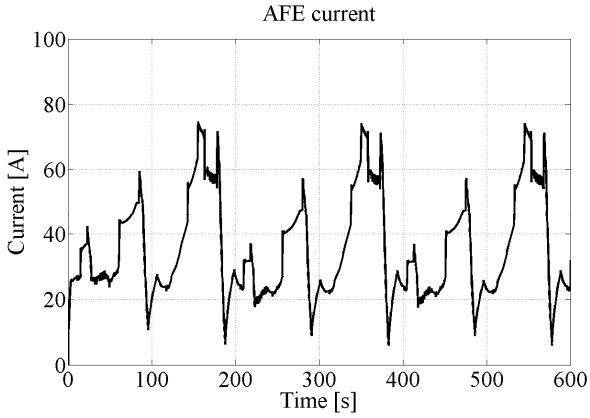


Fig. 14 The simulated AFE current, in case I, during three rounds of ECE cycle.

The simulated energy storage's voltage is shown in fig. 15. In simulation case I, the energy storage's capacitance was assumed to be 31,5 Farads and the ESR 34 mΩ.

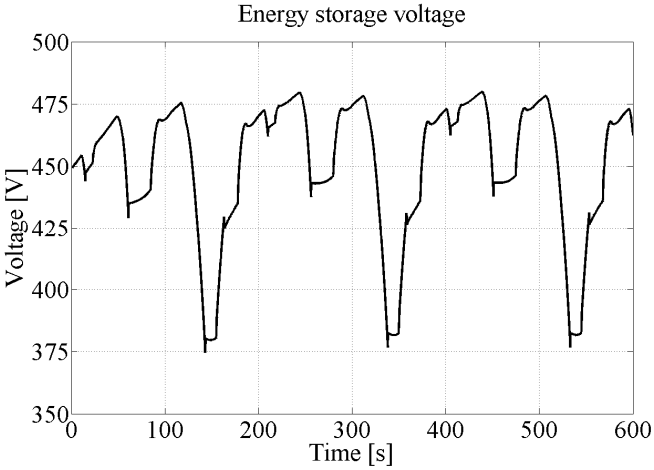


Fig. 15 The simulated supercapacitor module voltage, in case I, during three rounds of ECE cycle.

The dc link voltage was regulated in the simulations with the AFE, which got controls as a voltage reference and as a feedforward power transfer value. The simulated dc link voltage value is presented in fig. 16. In the simulations, the dc link capacitance was chosen to 40 mF, which directly affects to the variation of the dc link voltage.

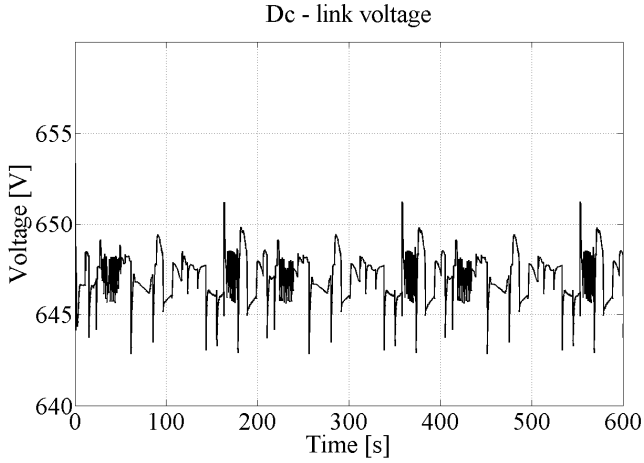


Fig. 16 The simulated dc link voltage, in case I, during three rounds of ECE cycle.

### 4.1.1.2 Simulations with the New European Driving Cycle

Next, the simulation results with the NEDC after 800 seconds are shown.

Figure 17 shows the dc/dc converter current during sub-urban part of the NEDC. In the end of the simulation figure can be seen the current spike, which is caused by energy storages voltage drop.

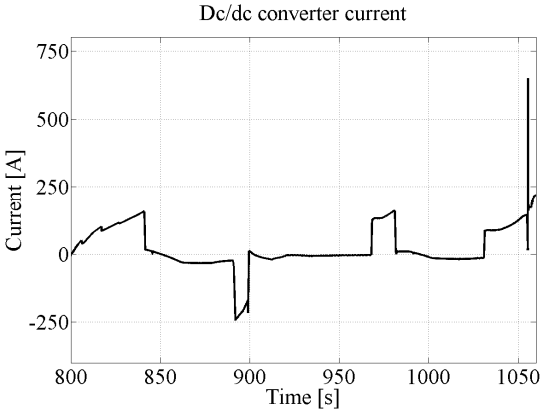


Fig. 17 The simulated dc/dc converter current, in case I, during NEDC sub-urban part.

The figure 18 shows the energy storages voltage, which causes failure of the simulated series hybrid power transfer during sub-urban part of NEDC. From the figure we can see that energy storages voltage drops to zero after 1050 secons of simulation.

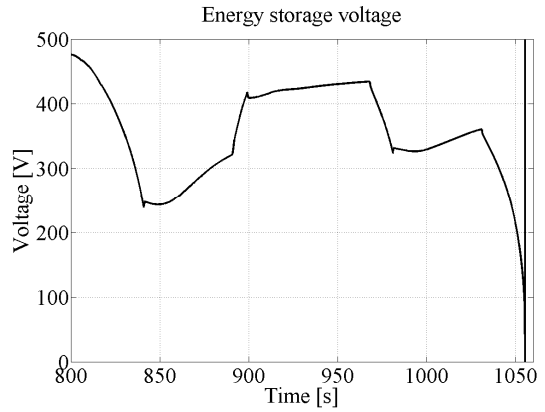


Fig. 18 The simulated supercapacitor module voltage, in case I, during NEDC sub-urban part.

## 4.2 The simulation figures with Braunschweig driving cycle

Simulations with the Braunschweig driving cycle were performed as NEDC. Following are shown simulation figures from control variables during Braunschweig driving cycles. Here only 400 seconds are shown to make pictures clearer, although results are obtained with 1800 seconds simulation. Fig. 19 represents the total load current, which was solved from Braunschweig driving cycle and from the constant power consumption.

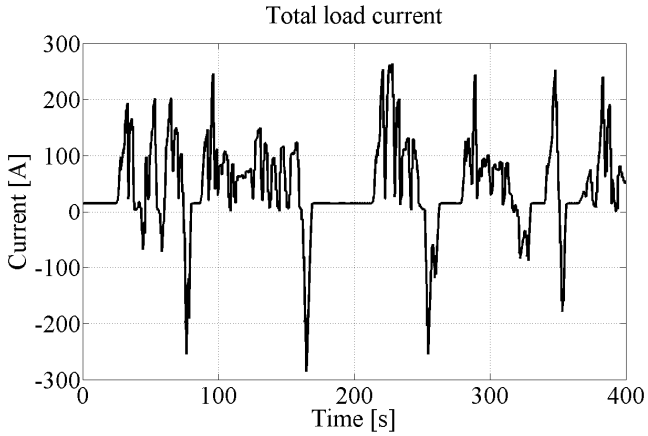


Fig. 19 The simulated load current, which was solved from the traction power and from constant power consumption for the 400 first seconds.

Fig. 20 shows the dc/dc converter current in the ES voltage level.

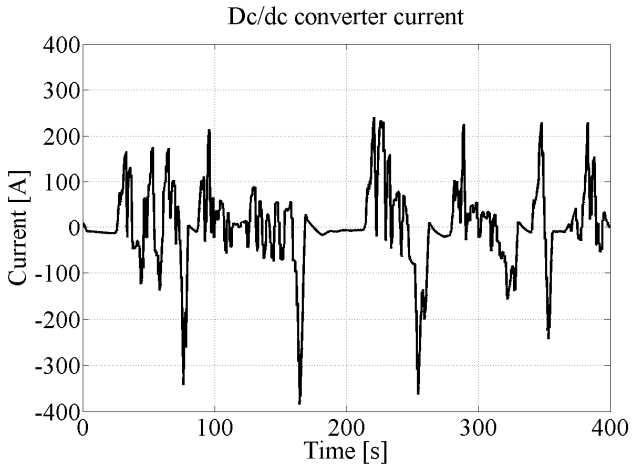


Fig. 20 The simulated dc/dc converter current, in case I, with Braunschweig driving cycle.

The active front end converter current was result of low-pass filtered power – flow control and regulation of the dc link voltage. The AFE current is shown in fig. 21.

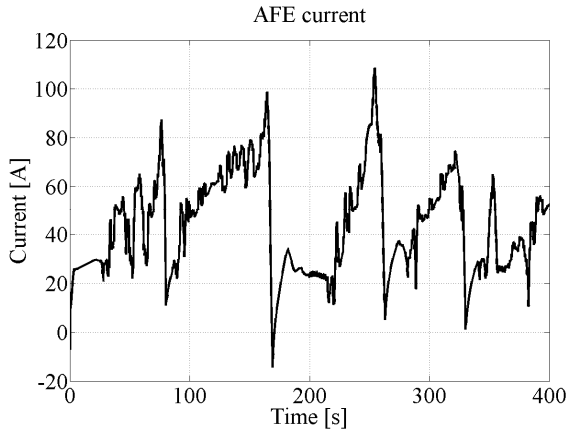


Fig. 21 The simulated AFE current, in case I, in the beginning of Braunschweig driving cycle.

In the Braunschweig driving cycle the ES voltage varied almost between nominal and half of the nominal value. This can be seen from fig. 22.

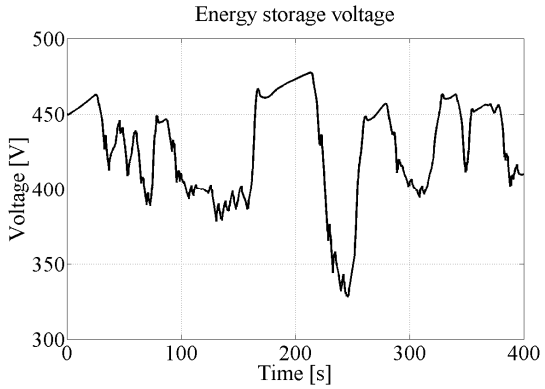


Fig. 22 The simulated supercapacitor module voltage, in case I, with the Braunschweig driving cycle.

The dc link voltage, which was also one of the control variables in the proposed control, is shown in fig. 23.

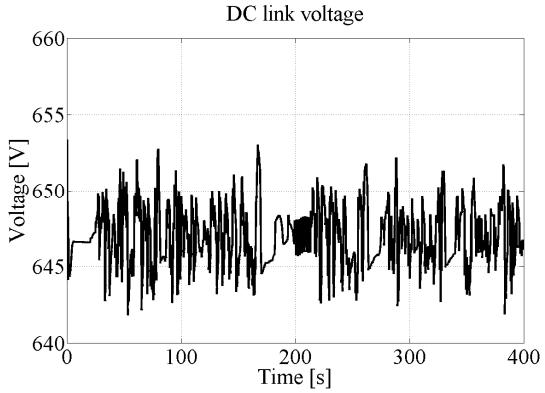


Fig. 23 The simulated dc link voltage, in case I, with the Braunschweig driving cycle.

## 4.3 The simulation results for both driving cycles

Following tables IV and V present the simulation results from the ECE and the Braunschweig cycles low-pass power filtering. These tables consists data from peak power decrease of the primary energy source, energy losses during low-pass power filtering and rating of dc/dc converter and supercapacitor module.

The maximum propulsion power in ECE cycle was 96,2 kW, which includes both the traction power and the constant power consumption. Similar value for the Braunschweig cycle is 156 kW.

TABLE IV

Simulation results with 4 rounds of ECE cycle

| Quantity | Case I | Case II | Case III |
|---|---|---|---|
| Maximum power from the VSDG, [%] of the maximum load | 60,9 % | 59,9 % | 59,4 % |
| Energy losses in the dc/dc converter, average value during 4 simulation rounds | 525 Ws | 684 Ws | 693 Ws |
| Energy losses in the supercapacitor ESR | 230,1 Ws | 353 Ws | 209 Ws |
| ES maximum current | 156 A | 158 A | 155 A |
| ES rms current | 31,3 A | 31,0A | 31,7 A |
| Voltage after 4 ECE cycles | 439 V | 333 V | 328 V |

| | Case IV | Case V |
|---|---|---|
| Maximum power from the VSDG, [%] of the maximum load | 72,6 % | 60,3 % |
| Energy losses in the dc/dc converter, average value during 4 simulation rounds | 542 Ws | 517 Ws |
| Energy losses in the supercapacitor ESR | 526 Ws | 215 Ws |
| ES maximum current | 157 A | 157 A |
| ES rms current | 31,2 A | 31,4 A |
| Voltage after 4 ECE cycles | 524 V | 506 V |

TABLE IV

Simulation results of Braunschweig cycle

| Quantity | Case I | Case II | Case III |
|---|---|---|---|
| Maximum power from the VSDG, [%] of the maximum load | 53,4 % | 60,0 % | 50,8 % |
| Energy losses in the dc/dc converter, average value during 4 simulation rounds | 910,2 Ws | 1235 Ws | 1120 Ws |
| Energy losses in the supercapacitor ESR | 628 Ws | 1043 Ws | 579 Ws |
| ES maximum current | 387 A | 400,0 A | 383 A |
| ES rms current | 55 A | 54,9 A | 55,4 A |
| Voltage after 4 ECE cycles | 429 V | 316 V | 313 V |

| | Case IV | Case V |
|---|---|---|

| | | |
|---|---|---|
| Maximum power from the VSDG, [%] of the maximum load | * | 54,4 % |
| Energy losses in the dc/dc converter, average value during 4 simulation rounds | * | 883 Ws |
| Energy losses in the supercapacitor ESR | * | 573 Ws |
| ES maximum current | * | 390,0 A |
| ES rms current | * | 54,9 A |
| Voltage after 4 ECE cycles | * | 495 V |

* The energy storages' voltage dropped to zero with the proposed control parameters.

The performed simulations suggest that in urban areas and with very cyclic driving cycles it is possible to decrease peak powers to half of their original values. This peak power reduction can be done with several ways. The proposed low – pass filtered power flow control efficiency is dependent from the control parameters and from the dimensions of the energy storage. By increasing the amount of series coupled supercapacitor cells we can decrease energy losses in the dc/dc converter and in the ES. On the other hand, by paralleling supercapacitor cells or modules, we can decrease energy losses in the energy storage. Paralleling of supercapacitors naturally increases the capacity of the energy storage, which affects the stability of the power – flow control and also to the energy losses of the dc/dc converter.

# 5 Conclusion

The simulations suggest that the low-pass power control can achieve near 50 % down rating of the maximum power from the primary energy source, while in same time the energy storage's voltage fluctuates within 50 % of its maximum value. Previous conclusion is related to vehicles that are moving only in urban areas or have very frequent accelerating decelerating cycles. The low-pass power-flow control is not that effective when changed to sub-urban areas, where high power demand for energy storage charging and for traction purposes together comes with the delay. In cases of higher power peaks, as in sub-urban area driving cycles, more capacitance in energy storage is needed.

Simulations with different driving cycles suggest that the highest decrease for the primary energy source peak power is achieved in driving cycle with short accelerations and decelerations. Previous conclusion can be made by comparing simulation results from ECE, NEDC and Braunschweig driving cycles.

Energy losses generated by the low – pass power filtering algorithm is depended on the control parameters and from the dimensions of the supercapacitor module. Simulations clearly showed the benefit of paralleling supercapacitor modules, which decreases the ESR, and thereby the losses in the supercapacitor module. Also, the maximum operation voltage of the supercapacitor module showed its expected advantage when dc/dc converter energy losses are considered.

As a drawback, in the simulations, proposed control algorithm couldn't manage the peak power of the NEDC when driving cycles speed achieved 120 km/h. In addition, in this control algorithm the VSDG is used to charge the energy storage, which leads to unwanted generation of power transfer losses. However, this study was made to demonstrate possibilities to cut peak power values from the primary energy source.

In the case of Fuel Cell (FC) based systems, the very high cost of FC stacks makes it very important to reduce their nominal power [2]. This also can be achieved by low-pass filtered power flow control with long time constant, when only average power of the load is supplied to the dc link.

# 6 Acknowledgements

This study has been carried in HybDrive and HybLab projects financed by TEKES and TKK/MIDE, respectively.

## References

[1] I. Husain, *Electric and Hybrid Vehicles, Design Fundamentals*. CRC Press LLC, the United State of America, 2003.

[2] M. Ceraolo, A. Donato, G. Franceschi, "A General Approach to Energy Optimization of Hybrid Electric Vehicles", *IEEE Trans. on Vehicular Technology*, Vol 57, pp. 1433-1441, May 2008.

[3] M. Liukkonen, A. Hentunen, J. Suomela, J. Kyyrä, "Functional Simulations of Power Electronics Components in Series-Hybrid Machinery for the needs of OEM", *Nordic Workshop on Power and Ind. Electronics*, Jun. 2008.

[4] H. Yoo, S. K. Sul, Y. Park, J. Jeong "System Integration and Power-Flow Management for a Series Hybrid Electric Vehicle Using Supercapacitors and Batteries", *IEEE Trans. on Industry Applications*, Vol 44, pp. 108-114, Jan.-Feb. 2008.

[5] C. Andersson, "Observations on Electric Hybrid Bus Design", *Licentiate thesis, Dep. of Ind. Electrical Eng., Lund University*, pp. 65-80, 2001.

[6] R. Barrero, X. Tackoen, J. Van Mierlo, "Analysis and configuration of supercapacitor based energy storage system on-board light rail vehicles", *EPE-PEMC 2008 conference*, pp. 1512-1517, 1 – 3 Sept. 2008.

[7] Y. Cheng, J. Van Mierlo, P. Lataire, G. Maggetto, "Test Bench of Hybrid Electric Vehicle with the Super Capacitor based Energy Storage", *IEEE International Symposium on Ind. Elec.*, pp. 147-152, 4 – 7 Jun. 2007.
[8] Y. Cheng, J. Van Mierlo, P. Van den Bossche, P. Lataire, "Energy Sources Control and Management in Hybrid Electric Vehicles", *EPE-PEMC 2006 conference*, pp. 524-530, Aug. 2006.
[9] Y. Cheng, J. Van Mierlo, P. Van den Bossche, P. Lataire, "Super Capacitor based Energy Storage as Peak Power Unit in the Applications of Hybrid Electric Vehicles", *The 3rd IET International Conference on Power Elect., Machines and Drives*, pp. 404-408, Mar. 2006.
[10] M. J. Kim, H. Peng, "Combined control/plant optimization of fuel cell hybrid vehicles", *Proceedings of the American Control Conference*, pp. 496-501, Jun. 2006.
[11] J. Bauman, M. Kazerani, "A Comparative Study of Fuel-Cell-Battery, Fuel-Cell-Ultracapacitor, and Fuel-Cell-Battery-Ultracapacitor Vehicles", *IEEE Trans. On Vehicular Technology*, vol. 57, no. 2, pp. 760-769, Mar. 2008.
[12] J. Leuchter, V. Řeřucha, Z. Krupka, P. Bauer, "Dynamic Behavior of Mobile Generator Set with Variable Speed and Diesel Engine", *IEEE Conf. Power Electronics Specialists*, pp. 2287-2293, Jun. 2007.
[13] E-M Isola, J. Kyyrä, M. Bergelin, J. Keskinen, "Models of Supercapacitors and Their Charging Behavior", *IEEE Conf. P E Sp*, pp. 2x-2y, Jun. 2007.
[14] Z. Chlodnicki, W. Koczara, N. Al-Khayat, "Control Strategies of the Variable Speed Generating Systems", *IEEE Conf. EUROCON 2007*, pp. 1301-1309, Sep. 2007.
[15] Maxwell Product Guide, http://www.maxwell.com, Maxwell Technologies SA, Switzerland, 2009.
[16] E. Schaltz, A. Khaligh, P. O. Rasmussen, "Investigation of Battery/Ultracapacitor Energy Storage Rating for a Fuel Cell Hybrid Electric Vehicle", *IEEE Conf. Vehicle Power and Propulsion*, Sep. 2008.

# 7 Authors

**Matti Liukkonen** is an undergraduate with nearly finished M.Sc. (Eng.) degree in electrical engineering from the Helsinki University of Technology (HUT), Espoo, Finland.

In 2008, he wrote his master's thesis from "Functional Simulations of Power Electronics Components in Hybrid Machinery".

Since 2007, he has been working as research assistant in a project related to simulation and control of series hybrid power transfer in HUT.

From 2005 to 2007, he was working as a research assistant in R&D department in ABB, Drives Oy, Finland, and also in Corporate Research, ABB Switzerland Ltd.

**Ari Hentunen** received his M.Sc. degree in electrical engineering from the Helsinki University of Technology (HUT), Finland, in 2005. From 2005 to 2007, and since 2008, he has been working as a researcher at HUT. During 2007–2008 he worked at Patria Land & Armament as an R&D engineer in the field of model-based software development. His main research projects are in the field of hybrid electric work machines and DC/DC converters.

**Jussi Suomela** is senior research scientist and project manager in Department of Automation and Systems Technology in Helsinki University of Technology TKK since 1992. His main research areas are hybrid electric vehicles and field and service robotics. He received his doctoral degree from TKK in 2004.

**Jorma Kyyrä** (M'94) received the M.Sc., Lic.Sc., and D.Sc. degrees from Helsinki University of Technology (HUT), Espoo, Finland, in 1987, 1991, and 1995, respectively.

He has worked at the university since 1985 in various positions. Since 1996, he has been Associate Professor of Power Electronics and since 1998 Professor of Power Electronics. His research interests include power converters, modelling of converters, power factor correction, and distributed power systems. He is the Director of the Institute of Intelligent Power Electronics, IPE, HUT, Executive Director of the Research Foundation, HUT, since 2003.

Dr. Kyyrä was Vice-Chairman of the Finland Section from 1995 to 2004 and since 2003 has been a Board Member of the IEEE Nordic Education Chapter.

In 2008, he was nominated as Dean of Faculty of Electronics, Communications and Automation, in Helsinki University of Technology.